Hindawi
Advances in Materials Science and Engineering
Volume 2017, Article ID 4247217, 11 pages
https://doi.org/10.1155/2017/4247217

Research Article

Deterioration and Microstructural Evolution of the Fly Ash Geopolymer Concrete against $MgSO_4$ Solution

Tao Long,[1,2] Qingyuan Wang,[1,3] Zhongwei Guan,[2,3] Yu Chen,[3] and Xiaoshuang Shi[1]

[1]*Sichuan Provincial Key Laboratory of Failure Mechanics and Engineering Disaster Prevention & Mitigation, College of Architecture & Environment, Sichuan University, Chengdu 610065, China*
[2]*School of Engineering, University of Liverpool, Brownlow Hill, Liverpool L69 3GQ, UK*
[3]*School of Mechanical Engineering, Chengdu University, Chengdu 610106, China*

Correspondence should be addressed to Qingyuan Wang; wangqy@scu.edu.cn and Xiaoshuang Shi; shixs@scu.edu.cn

Received 9 June 2017; Revised 3 September 2017; Accepted 12 September 2017; Published 16 October 2017

Academic Editor: Giorgio Pia

Fly ash geopolymer concrete (FAGC) and ordinary Portland cement concrete (OPCC) specimens were immersed in 5% $MgSO_4$ solution undergoing 32 wetting-drying and heating-cooling cycles. Their compressive behavior was investigated after every 8 cycles. Several microstructure analysis techniques were applied on the samples to identify the materials formed due to magnesium sulfate attack, including XRD, FTIR, SEM, and EDS. Experimental results elucidated that the compressive strength loss ratio in the heating group of FAGC was 12.7%, while that of OPCC was 17.8%, which means that FAGC had better magnesium sulfate resistance than OPCC. The compressive strength loss of OPCC was due to the formation of gypsum under the magnesium sulfate attack exposed to wetting-drying and heating-cooling cycles. The deterioration mechanisms of FAGC against $MgSO_4$ solution were discovered to be that sodium aluminum silicate hydrate (N-A-S-H) gels reacted with $MgSO_4$, leading to the creation of low strength magnesium aluminum silicate hydrate (M-A-S-H) gels.

1. Introduction

Geopolymer concrete has increasingly attracted attention due to its environmentally beneficial applications as the process of alkali activation will utilize the industrial refuse such as fly ash and slag to reduce greenhouse gas emissions. It is well known that geopolymers exhibit high early age strength, low penetrability, and good fire resistance due to their greatly cross-linked triaxial aluminosilicate structure [1, 2]. Hence, they are regarded as a new alternative binder to replace ordinary Portland cement (OPC). Besides, sulfate attack on concrete is a major aggressive environmental deterioration, which affects the long-term durability of civil infrastructures. This is because when these infrastructures are exposed to sulfate industrial wastewater and ocean environments and saline-alkali land, the reaction between concrete and sulfate could induce cracking, spalling, or expansion of structures, further degrading their mechanical strength [3]. The rate and mechanism of sulfate attack on concrete depend on many factors, including the cation accompanying the sulfate ions, permeability, paste chemistry, and aggregate mineralogy. The mechanism of $MgSO_4$ attack on OPC is that the composite layers of $Mg(OH)_2$ and $CaSO_4$ are generated on the surface region, and in the inner zone near the surface, calcium silicate hydrate (C-S-H) tends to be exhausted in Ca [4, 5].

Nevertheless, the investigation on the sulfate exposure in FAGC is limited up till now. Some previous research reports [6–9] concluded that geopolymers are more durable than OPC under sulfate attack as the cross-linked aluminosilicate polymer structure is steadier than calcium silicate hydrate gel. C-S-H phases tend to react with $MgSO_4$ solution to constitute ettringite and gypsum, while the Na-Al-Si-H cross-linked structure of geopolymers resists sulfate corrosion. There are two different opinions on the sulfate attack mechanism of geopolymers. Some scholars [6, 8, 10] suggested that the deterioration of geopolymers in sulfate solution was due to the removal of hydroxyl ions from the matrix into the solution, as a remarkable increase in pH value was observed in the immersion solution accompanied by a largely decreased

mechanical strength of the specimen measured. Baščarević et al. [11] approved the first opinion by using nuclear magnetic resonance, claiming that the settlement of geopolymeric samples with the SO_4^{2-} solution caused the destruction of silicon-oxygen-silicon bonds in $x Al_2O_3 \cdot y SiO_2$ gel structure. Both destruction of the silicon-oxygen-silicon bonds and extracting of silicon were responsible for the enhancement of hydroxide ion concentration of the sulfate solution during the experiment. The second opinion was proposed by Ismail et al. [12]. They claimed that the degradation of geopolymers is not due to the sulfate itself, but to the cation accompanying the sulfate anions, since the massive material degradation of the mortars was found during being immersed in $MgSO_4$ solution, but not in Na_2SO_4 solution. The presence of Mg leads to the migration of Ca^{2+} from the calcium-rich gels in the geopolymer matrix, but sodium does not have this kind of function. In addition, the partial substitute of fly ash by metakaolin [13] and higher Na_2O content [14] can contribute to improving the sulfate resistance of geopolymer specimens. This is because the metakaolin substitution and Na_2O addition are associated with each other to form an optimal microstructure, which impedes the damage of the matrix by sulfate attacks. It is well known that the resistance to sulfate attack is highly correlated with the dense microscopic structure and the high compressive strength. Chindaprasirt et al. [15] demonstrated that the microwave-heated high calcium fly ash geopolymer has a lower strength loss under sulfate attacks compared with the conventional heat cured samples.

In sulfate environment, structures located in water-level fluctuation, littoral area, and spray zone will experience more complicated environmental damage through the drying-wetting cycles, which tends to deteriorate the concrete more rapidly [16]. Jiang and Niu [17] proved that the degree of degradation of OPC concrete in $MgSO_4$ solution under drying-wetting cycles was more rigorous than that only immersed in the same sulfate solution without drying-wetting cycles. Sahmaran et al. [18] suggested that, for the structures subjected to sulfate solution under the wetting-drying and heating-cooling cycles, the sulfate resistant Portland cement was observed to achieve better compressive strength losses than blended cement.

However, the pattern of sulfate attack which is chosen by most researchers for geopolymers is immersion [19, 20]. Few literatures presented the property of FAGC subjected to the sulfate attack under drying-wetting and heating-cooling cycles, which could expedite the deterioration process of concrete. Therefore, this research reported an observation of both the compressive behavior and the microstructural characteristics of FAGC. It revealed the performance deterioration mechanism of the concrete in the $MgSO_4$ solution under drying-wetting and heating-cooling cycles.

2. Experiment Procedure

2.1. Materials. Fine and coarse aggregate, OPC (PO 42.5R, Sichuan Lanfeng Cement Limited Company, China), fly ash (Class F, Tianjin Dagang Power Plant), alkaline activating solution, and magnesium sulfate solution were used as raw materials for the experimental work. The properties of aggregates and the chemical constitutions of OPC and fly ash are shown in Tables 1 and 2, respectively. The gradation curves for aggregates and fly ash are shown in Figure 1. The alkaline activating solution contained Na_2SiO_3 and NaOH. The chemical compositions of the Na_2SiO_3 solution (Foshan Zhongfa Water Glass Factory) were Na_2O (8.83%), SiO_2 (27.64%), and H_2O (63.53%) by mass. NaOH solution was prepared by distilled water to provide 10 mol/L concentration. The pH value of the final alkaline activating solution was 13.3 by using model 8601 pH meter. The concentration of magnesium sulfate solution was 5% by mass, and the pH of magnesium sulfate solution was 7.

2.2. Specimen Preparation. Two mixtures were projected to compare the property of OPCC and FAGC exposed to sulfate solution. The concrete mixture ratio designs are outlined in Table 3. OPCC was demolded after being cast by 24 hours and cured in a standard condition of 20 ± 2°C and 95% relative humidity for 28 days. The alkali-activated solution was prepared one day prior to the mixing of the geopolymer concrete. The mixing of the geopolymer concrete was completed in a pan mixer. Dry coarse/fine aggregates and fly ash were mixed in the mixer for about 3 minutes. The prepared alkali-activated solution was then sequentially added and the wet mixing was continued for another 5 minutes. Before casting, the inner sides of the mold were layered with lubricating oil to prevent adhesion with the geopolymer concrete specimens. The molds were filled in three layers, and each layer was well compacted. The molds were vibrated for about one minute on the vibration table. FAGC was cured at 80°C for 24 hours after casting, followed by curing under the same standard condition with the OPCC specimens for 28 days.

2.3. Testing Procedures

2.3.1. Cyclic Test and Compression Strength Test. The drying-wetting and heating-cooling processes were performed on the concrete sulfate drying-wetting test machine (CABR-LSB, China Academy of Building Research Co., Ltd., China). The duration of one cycle was 24 hours. The drying-wetting and heating-cooling cycles were carried out as follows. At first, the specimens were soaked for 14 hours, with the temperature of the solution being set as 20°C. This was followed by 5 hours of drying with 80°C heating. Then, the samples were kept for 5 hours under 20°C cooling. The standard for the drying-wetting and heating-cooling test to be carried out for concrete was the standard for test methods of long-term performance and durability of ordinary concrete, GB/T 50082-2009, Test Method for Resistance of Concrete to Sulfate Attack. The procedure above was repeated for 32 cycles. The compressive strength of specimens (100 mm × 100 mm × 100 mm cubes) was measured using an electrohydraulic servo controlled compression test machine (YAW-2000, Changchun New Testing Machine Co., Ltd., China) with a loading capacity of 2000 kN, before the exposure test and at every 8 cycles. The loading rate during the compression tests was 5 kN/s.

Table 1: Properties of aggregates.

Category	Bulk density (kg/m^3)	Apparent density (kg/m^3)	Moisture content (%)	Maximum particle size (mm)	Average particle size (mm)
Coarse aggregate	1479	2632	0.3	22	12.38
Fine aggregate	1342	2381	0.1	4	0.33

Table 2: Chemical compositions of OPC and fly ash.

	SiO_2	Al_2O_3	CaO	Fe_2O_3	MgO	K_2O	P_2O_5	TiO_2	Na_2O	LOI
OPC	18.63	2.49	71.70	2.62	3.24	0.48	/	0.84	/	4.75
Fly ash	74.18	9.44	5.53	4.22	2.48	1.46	1.41	0.96	0.32	0.82

The value presented is the weight percentage. LOI: loss on ignition.

Table 3: The concrete mixture ratio designs (kg/m^3).

Mixture	Gravel	Sand	Fly ash	Cement	NaOH solution	Na_2SiO_3 solution	Water	W/G ratio
OPCC	1208	592	—	400	—	—	200	0.5
FAGC	1318	647	437	—	62	156	—	0.5

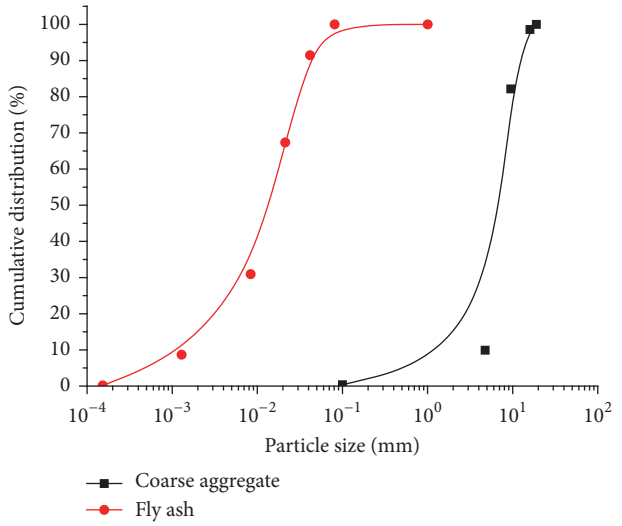

Figure 1: The gradation curve of fly ash and coarse aggregate.

The mass of samples (100 mm × 100 mm × 400 mm) was measured by an electronic balance before the exposure test and at every 8 cycles.

2.3.2. Structural Characterization. The surfaces (0-1 mm depth) of the chosen specimens were inspected with XRD, FTIR, SEM, and EDS. XRD analysis was performed on EMPYREAN (PANalytical B.V., Holland), scanning from 5° to 65° 2θ. FTIR analysis was made with Nicolet 6700 (Thermo Electron Corporation, USA) in the range of 400–4000 cm^{-1}. Thermogravimetric analysis was carried out by TGA/DSC2 (Mettler-Toledo, Switzerland), at a heating rate of 20°C/min with the range of 25–1000°C. SEM and EDS analyses were carried out by using S4800 (Hitachi, Japan) equipped with an EDS analyzer (Oxford Image Analysis).

3. Results and Discussion

3.1. Visual Observation. There were no obvious visual changes of OPCC and FAGC specimens after 32-cycles drying-wetting and heating-cooling sulfate attack. The surface of the samples had no deposits and was as smooth as before the test, as shown in Figure 2.

3.2. Compression Strength Evolution. The consequences from the compression strength development of OPCC were presented in Figure 3. As could be seen in the histogram, the initial strength of OPCC exhibited a value of 43.5 MPa. In the standard curing environment, it steadily rose to 51 MPa after 60 days, with an increase of 17.2% compared to the initial strength. Due to the $MgSO_4$ solution attack, the compression strength of specimens was clearly lower than that in the standard curing environment with the same age. Also, the compressive strength of OPCC specimens after 32-cycle attack was mildly higher than that of OPCC samples after 24-cycle attack, which resulted from corrosion deposits being formed in the microcosmic pore structures to make the binder denser [17]. The outcomes revealed that the $MgSO_4$ attack contributed to the reduction of the compressive strength of OPCC.

The variation in the compression strength of FAGC with time is exhibited in Figure 4. From the figure, it is clear that the initial compression strength (28 days) of FAGC was 32 MPa, with some fluctuations on the strength for

Figure 2: The visual appearance of OPCC and FAGC specimens before and after sulfate attack.

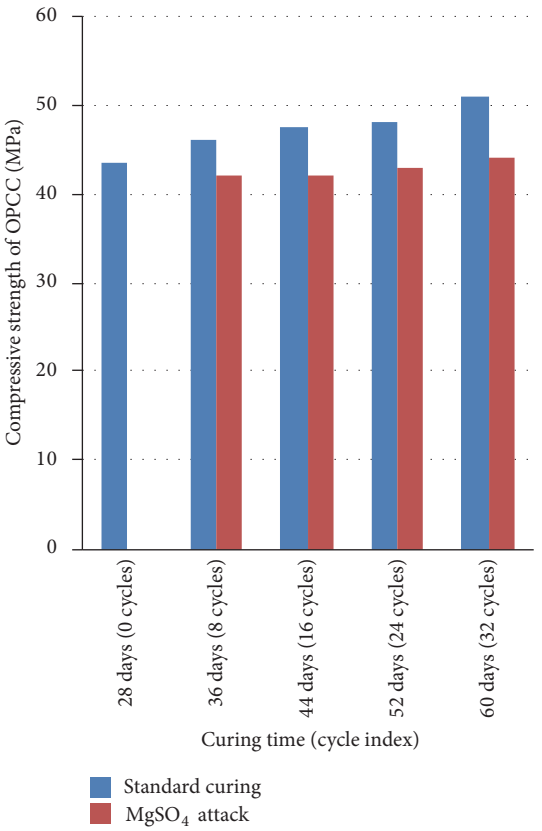

Figure 3: Compression strength evolution of OPCC in the standard curing condition and $MgSO_4$ attack, respectively.

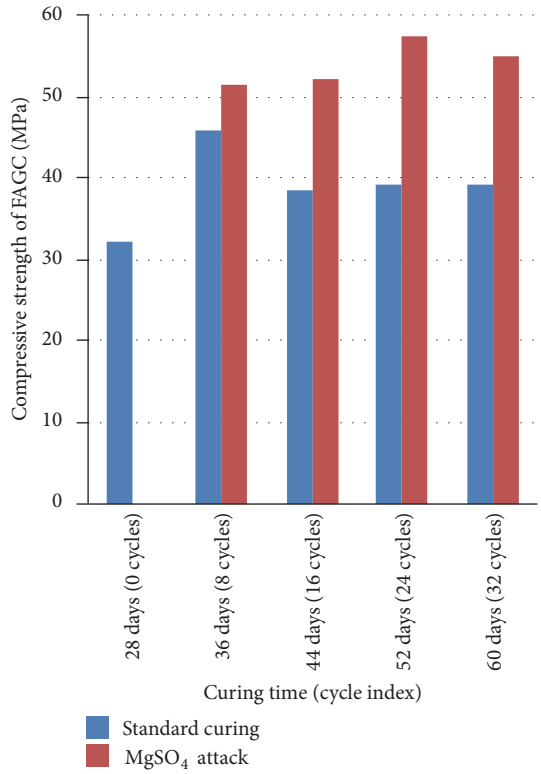

Figure 4: Compression strength evolution of FAGC in the standard curing condition and $MgSO_4$ attack, respectively.

both the standard curing condition and the $MgSO_4$ attack. The compressive strength of FAGC in the standard curing condition increased by 21.88% after 60 days, but it soared by 71.88% in the $MgSO_4$ attack after 32 cycles. The compressive strength of FAGC after $MgSO_4$ attack was higher than that of FAGC in standard curing condition with the same age. Bakharev [6] also found that, in the magnesium sulfate solution for 30 days, 16.7% increase in strength was measured in the geopolymers manufactured by low Ca fly ash and NaOH solution.

As demonstrated in Figures 3 and 4, the results revealed that OPCC samples suffered strength loss but FAGC specimens gained strength increase after $MgSO_4$ attack. Sumajouw et al. [21] concluded that, with the maintenance temperature rising in the scope from 30 to 90°C, the compressive strength of geopolymeric concrete increased. Besides, a longer maintenance time, in the scope from 6 hours to 3 days, exhibited a higher strength of compression for geopolymer concrete. The heating temperature improved the polymerization reaction process, which made fly ash and alkali-activated solution constitute the matrix in the early stage [22]. To prove whether the magnesium sulfate solution deteriorates the geopolymer concrete or not, this research added a heating group. The test procedure of this heating group was to make the specimens experience the same duration (160 hours) of heating as the 32-cycle $MgSO_4$ attack samples do, with the heating group being cured in the standard curing condition. Figure 5 shows the compressive strength of OPCC and FAGC specimens subjected to the 32-cycle $MgSO_4$ attack environment and in the heating group. The compression strength of FAGC specimens in the heating group was higher than that of the samples under 32-cycle $MgSO_4$ attack, which illustrated that fly ash geopolymeric concrete suffered strength loss in the magnesium sulfate attack.

The deterioration of heating group samples was explained by the compression strength loss ratio R^H, which was calculated using

$$R^H = \frac{f_{ch} - f_{c32}}{f_{ch}} \times 100\%, \quad (1)$$

where R^H is the compression strength loss ratio of heating group samples (%), f_{c32} is the compression strength of the experiment group specimens after 32 cycles, and f_{ch} is the compression strength of the heating group specimens.

By calculation, R^H of OPCC (17.8%) was higher than that of FAGC (12.7%). From the result, it was clear that FAGC had better magnesium sulfate resistance than OPCC, because the cross-linked aluminosilicate polymer structure of FAGC was firmer than the C-S-H gel of OPCC, which could be confirmed by the microstructure analysis results below.

3.3. Mass Change. The mass of both OPCC and FAGC specimens rose after the sulfate attack, as presented in Figure 6. The increase of OPCC specimens was 0.8% compared to the initial mass after 32-cycle drying-wetting and heating-cooling sulfate penetration. The mass growth rate of FAGC specimens was 4.05% after the same experiment period. The reason of the mass increase might be that water was still in the OPCC or FAGC specimens even after 10-hour heating and cooling. The results demonstrated that the water absorptivity of FAGC was stronger than that of OPCC.

3.4. Microstructure Analysis

3.4.1. XRD Analysis. The XRD patterns of OPCC in the 60-day standard curing condition, heating condition, and the 32-cycle $MgSO_4$ attack environment are presented in Figure 7. When OPCC specimens were exposed to $MgSO_4$ solution, quartz, calcium hydroxide, C-S-H gel, and gypsum could be observed in the peaks. The quartz, calcium hydroxide, and C-S-H could be the main hydration products, as their peaks are strong. Gypsum could be observed at around 32.14° (2θ), which demonstrated that gypsum was a corrosion product. Similar results were also suggested by Jiang and Niu [17] and Qi et al. [23]. Moreover, the peak of C-S-H in the specimen under 32-cycle $MgSO_4$ attack environment disappeared at about 27.57° (2θ), which meant that C-S-H reacted with $MgSO_4$ and the number of C-S-H gels decreased. The XRD analytical results agreed with the compressive strength of OPCC.

As shown in Figure 8, the main phases that could be detected were quartz and N-A-S-H gel. Traces of M-A-S-H gel could be observed at 8.60° (2θ) in the XRD spectrum of the 32-cycle $MgSO_4$ attack group, which illustrated that $MgSO_4$ reacted with N-A-S-H gel and produced M-A-S-H gel [12]. It was observed that the concentration of N-A-S-H gel in the

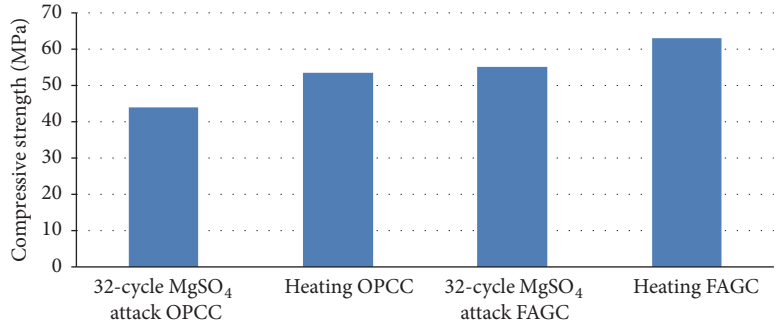

Figure 5: Compression strength of OPCC and FAGC specimens in the 32-cycle $MgSO_4$ attack and heating group.

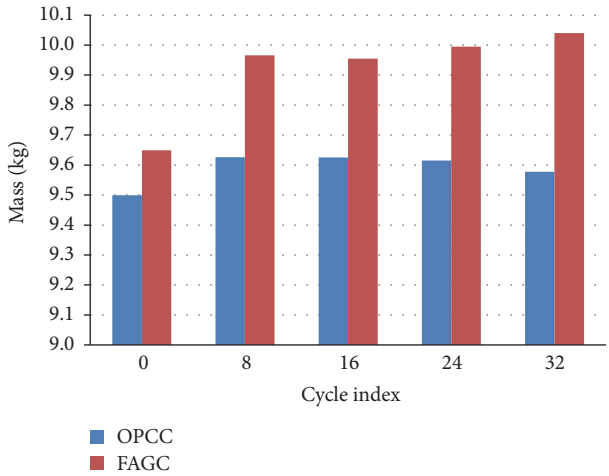

Figure 6: The mass change of OPCC and FAGC samples with the cycle index.

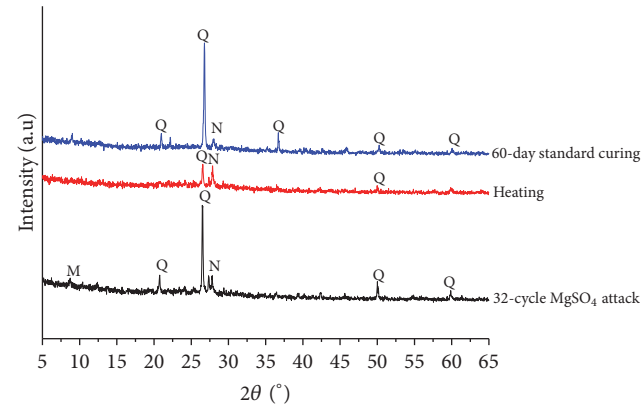

Figure 8: XRD patterns of FAGC in the 60-day standard curing condition, heating condition, and 32-cycle $MgSO_4$ attack environment, respectively. Q: quartz; N: N-A-S-H (sodium aluminum silicate hydrate); M: M-A-S-H (magnesium aluminum silicate hydrate).

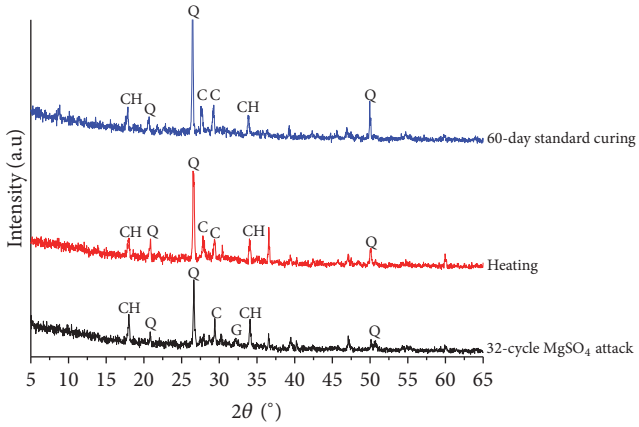

Figure 7: XRD patterns of OPCC in the 60-day standard curing condition, heating condition, and 32-cycle $MgSO_4$ attack environment, respectively. Q: quartz; CH: calcium hydroxide; G: gypsum; C: C-S-H (calcium silicate hydrate).

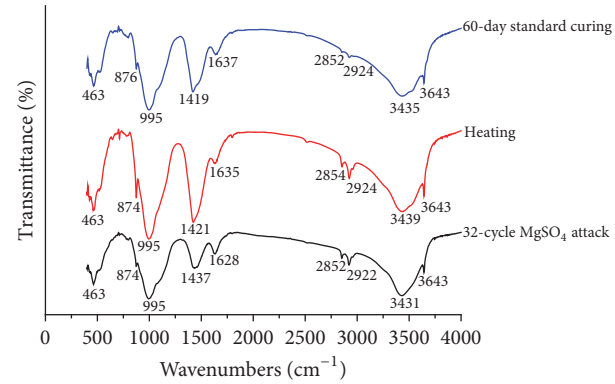

Figure 9: FTIR of OPCC in the standard curing condition of 60 days, heating condition, and 32-cycle $MgSO_4$ attack environment, respectively.

60-day standard curing group was lower than that of N-A-S-H gel in the heating and 32-cycle $MgSO_4$ attack group, which coincided with the compressive strength behavior of FAGC under magnesium sulfate attack.

3.4.2. FTIR Analysis. The FTIR spectra of OPCC samples under 60-day standard curing, heating, and 32-cycle $MgSO_4$ attack conditions are shown in Figure 9. The bands at about 874 and 1420 cm^{-1} meant existence of CO_3^{2-}, which indicated that the specimens had already attracted CO_2 molecules from the atmosphere before immersion into $MgSO_4$ solution [24].

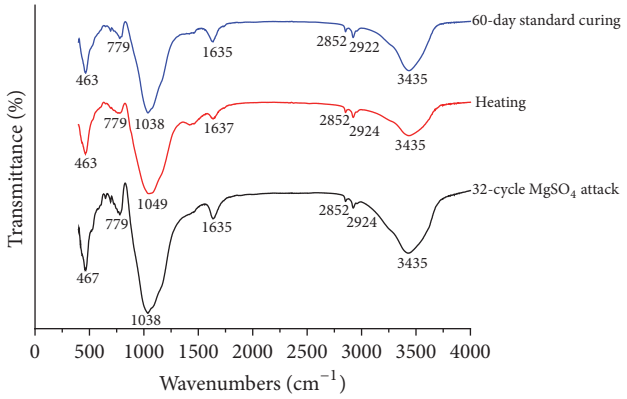

Figure 10: FTIR of FAGC in the 60-day standard curing condition, heating condition, and 32-cycle $MgSO_4$ attack environment, respectively.

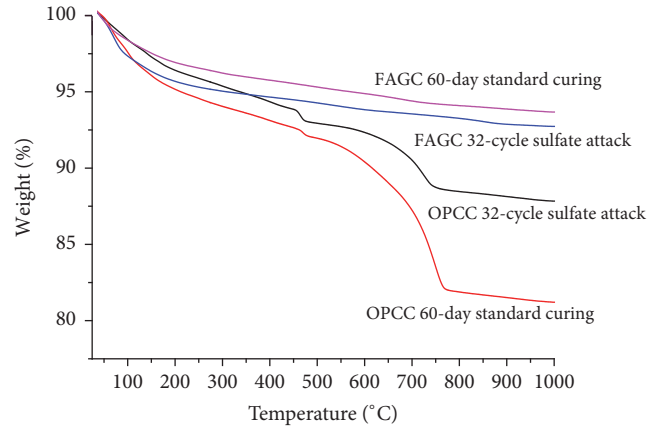

Figure 11: TGA results of OPCC and FAGC in the 60-day standard curing condition and 32-cycle MgSO4 attack environment.

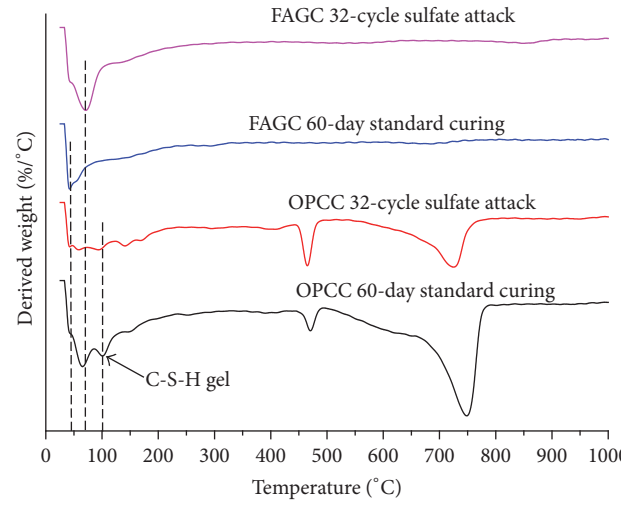

Figure 12: DTG results of OPCC and FAGC in the 60-day standard curing condition and 32-cycle MgSO4 attack environment.

The band of approximately 995 cm^{-1} came from asymmetric stretching vibration of silicon-oxygen bond in the hydrated calcium silicate gel [25]. It could be observed clearly from Figure 10 that the strength of the band at around 995 cm^{-1} in the 32-cycle $MgSO_4$ attack sample was lower than that in the samples under 60-day standard curing and heating conditions. This probably resulted from the degradation of hydrated calcium silicate gel caused by $MgSO_4$ attack. The band of approximately 3643 cm^{-1} was due to the stretching vibration of hydroxy bond in calcium hydroxide [6]. The bending vibration and stretching vibration of hydroxy bond in hydration products induced the changes in the bands at around 1630 and 3435 cm^{-1}, respectively [6]. The aluminum oxygen bond vibrations of $[Al(OH)_6]^{3-}$ resulted in the bands at around 463 cm^{-1} [26, 27].

As could be observed from Figure 10, there was no noticeable difference in the sample under the 60-day standard curing condition, heating condition, and 32-cycle $MgSO_4$ attack environment. In geopolymers based on fly ash, the band at about 1038 cm^{-1} came from asymmetric stretching vibration of Si-O-Al, demonstrating that alkaline activation caused the constitution of an alkaline aluminosilicate (N-A-S-H or M-A-S-H) gel with amorphous nature [28]. The feature located at 770 cm^{-1} was characterized as symmetric stretching vibration of Si-O-Si [29]. The vibrations attributed to bending and stretching of hydrogen bonds were investigated in about 1635 and 3435 cm^{-1}, respectively. The FAGC samples subjected to $MgSO_4$ attack under 32 drying-wetting and heating-cooling cycles still maintained the original structure, which indicated that the FAGC samples were durable to magnesium sulfate attack.

3.4.3. Thermogravimetric Analysis. The TGA results presented in Figure 11 showed that the mass loss observed was a little higher in FAGC specimens after exposure to $MgSO_4$, when compared with the standard curing FAGC samples. However, the mass loss of OPCC standard curing specimens was much higher than that of OPCC sulfate attack samples. The DTG results in Figure 12 indicated that, as for OPCC specimens, the peak near 100°C was mainly attributed to the dehydration of C-S-H gel. Compared to OPCC 60-day standard curing samples, sample OPCC 32-cycle sulfate attack had a weak strength of the peak for C-S-H gel, which was consistent with the XRD and FTIR results. In the FAGC samples, an endothermic peak was observed between 50°C and 70°C, which was attributed to the loss of evaporable water in the sample, and the water was combined in the aluminosilicates [30].

3.4.4. SEM and EDS Analysis. Specimens were adopted from the failed concrete of compression tests. Before being exposed to magnesium sulfate solution, typical reaction products of OPCC, such as crystalline $Ca(OH)_2$, floc, and fibriform hydrated calcium silicate gel, could be seen in Figure 13. From the EDS analysis, the major chemical product in the paste is C-S-H gel, in which Si and Ca took up the 32.30% and 8.94% weighting, respectively.

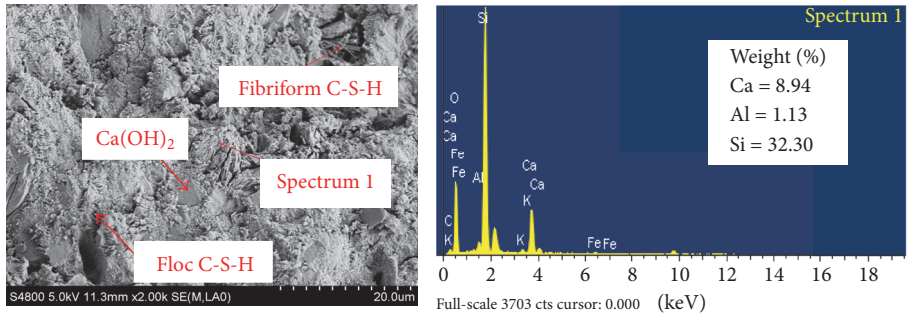

Figure 13: SEM and EDS results of OPCC in the 60-day standard curing group.

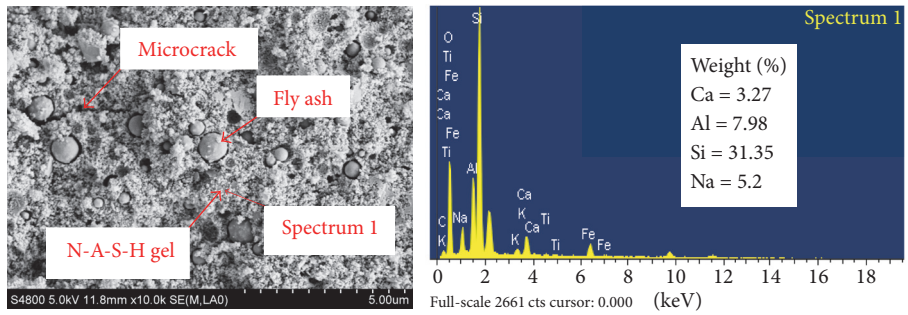

Figure 14: SEM and EDS results of FAGC in the 60-day standard curing group.

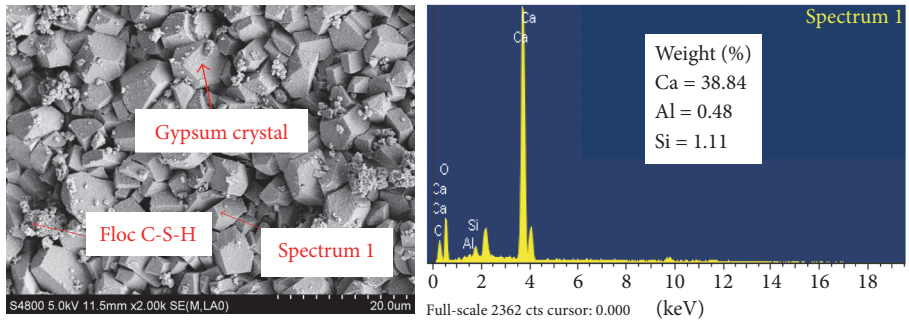

Figure 15: SEM and EDS results of OPCC in the 32-cycle $MgSO_4$ attack environment.

As for the FAGC group specimens with 60-day standard curing, numerous unreacted fly ash particles were discovered in the binder as shown in Figure 14. This suggested that fly ash fine particles did not react with the solution which led to the low 60-day compressive strength on the macroscale [31]. The amorphous N-A-S-H gel could be found, which was validated by the EDS result with 5% weight of Na, supporting XRD finding in Figure 8 and FTIR finding in Figure 10.

After 32 wetting-drying and heating-cooling cycles, many $CaSO_4 \cdot 2H_2O$ crystals could be discovered in the OPCC as shown in Figure 15. This suggested that decalcification or decomposition of hydrated calcium silicate and calcium hydroxide phase in the OPCC supplied the calcium required for the formation of gypsum. Gypsum was expansive and this expansion resulted in the development of internal stresses that could damage the concrete and lead to a reduction in strength [32]. Besides, only a small number of floc C-S-H gels were observed. Ettringite was unstable and could be decomposed when temperature exceeded 60–70°C [33], so it did not appear in the specimens in the 32-cycle $MgSO_4$ attack environment, which were exposed to heating-cooling environments.

The amorphous aluminosilicate gels in the FAGC group subjected to 32-cycle $MgSO_4$ attack were much denser in Figure 16 than those in the FAGC 60-day standard curing group in Figure 14. Therefore, the compression strength of the former was much higher than that of the latter. The results in the EDS analysis illustrated that amorphous aluminosilicate gels included the low strength magnesium aluminosilicate hydrate (M-A-S-H) gel [34], which gave an explanation on the decrease of compressive strength in comparison to the heating group. Compared with the FAGC 60-day standard

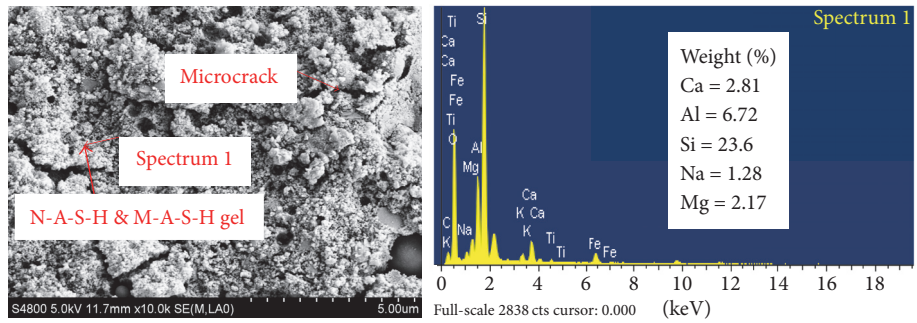

Figure 16: SEM and EDS results of FAGC in the 32-cycle $MgSO_4$ attack environment.

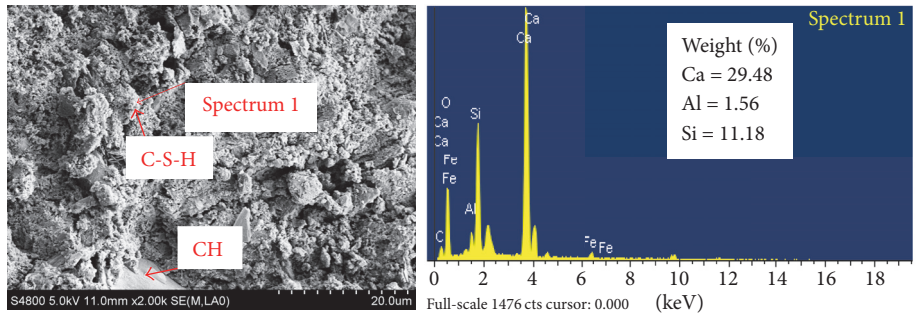

Figure 17: SEM and EDS results of OPCC in the heating group.

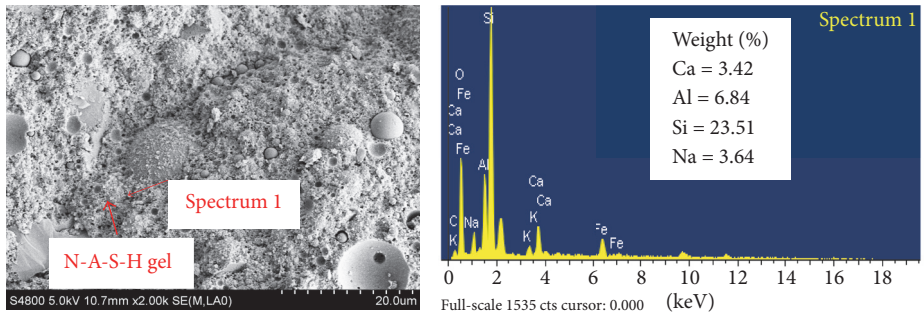

Figure 18: SEM and EDS results of FAGC in the heating group.

curing group, the weight of Na in the 32-cycle $MgSO_4$ attack group decreased from 5.2% to 1.28%, which gave a clarification that a few of N-A-S-H gels were decomposed.

The number of hydrated sodium silicate gels in the OPCC heating group samples in Figure 17 was a little more than that of hydrated sodium silicate gels in the OPCC 60-day standard curing group samples. Thus, the compressive strength in the OPCC heating group was slightly higher than that in the OPCC 60-day standard curing group.

The sodium aluminum silicate hydrate gels in the heating group in Figure 18 were a bit denser than those in the 32-cycle $MgSO_4$ attack group and no microcrack could be found compared with the 32-cycle $MgSO_4$ attack group samples. This might explain that the compression strength of heating specimens was a little higher than that of 32-cycle $MgSO_4$ attack specimens.

4. Conclusions

Based on the observation and analysis in the deterioration of FAGC subjected to magnesium sulfate solution with wetting-drying and heating-cooling cycles, some important parameters such as the compressive strength and microstructure characteristics were studied and analyzed using various analysis tools. Here, the main findings could be concluded as follows.

(i) Laboratorial outcomes demonstrated that the compressive strength loss ratio of OPCC and FAGC heating group specimens was 17.8% and 12.7%, respectively, after 32 wetting-drying and heating-cooling cycles. FAGC had better magnesium sulfate resistance than OPCC as the cross-linked aluminosilicate

polymer structure was more stable than hydrated calcium silicate gel after $MgSO_4$ attack.

(ii) Based on the consequences of XRD, FTIR, SEM, EDS, and TGA/DTG, the magnesium sulfate attack mechanism of OPCC could be explained as follows: $MgSO_4$ reacts with C-S-H and creates expansive and low strength gypsum with the decomposition of C-S-H. Besides, ettringite did not exist in the heating-cooling environment.

(iii) The heating-cooling regime enhanced the compressive strength of FAGC samples since polymerization reactions were highly temperature-dependent. The deterioration of FAGC under magnesium sulfate attack after 32 drying-wetting and heating-cooling cycles was due to N-A-S-H gels reacting with $MgSO_4$, which produced low strength M-A-S-H gels based on the microstructure analysis.

Conflicts of Interest

The authors declare that there are no conflicts of interest regarding the publication of this paper.

Acknowledgments

The authors are sincerely grateful for the financial support provided by the Program for Changjiang Scholars and Innovative Research Team of China (IRT14R37), National Natural Science Foundation of China (no. 51208325), and the Science & Technology Support Program of Sichuan Province (no. 2015GZ0245 and no. 2015JPT0001). The first author is supported by the China Scholarship Council (CSC), which is sincerely appreciated.

References

[1] J. L. Provis and J. S. J. Van Deventer, *Geopolymers: structure, processing, properties and industrial applications*, CRC, 2009.

[2] X. Y. Zhuang, L. Chen, S. Komarneni et al., "Fly ash-based geopolymer: Clean production, properties and applications," *Journal of Cleaner Production*, vol. 125, pp. 253–267, 2016.

[3] S. W. Tang, Y. Yao, C. Andrade, and Z. J. Li, "Recent durability studies on concrete structure," *Cement and Concrete Research*, vol. 78, pp. 143–154, 2015.

[4] D. Bonen and M. D. Cohen, "Magnesium sulfate attack on portland cement paste-I. Microstructural analysis," *Cement and Concrete Research*, vol. 22, no. 1, pp. 169–180, 1992.

[5] D. Bonen and M. D. Cohen, "Magnesium sulfate attack on portland cement paste - II. Chemical and mineralogical analyses," *Cement and Concrete Research*, vol. 22, no. 4, pp. 707–718, 1992.

[6] T. Bakharev, "Durability of geopolymer materials in sodium and magnesium sulfate solutions," *Cement and Concrete Research*, vol. 35, no. 6, pp. 1233–1246, 2005.

[7] A. Fernandez-Jimenez, I. García-Lodeiro, and A. Palomo, "Durability of alkali-activated fly ash cementitious materials," *Journal of Materials Science*, vol. 42, no. 9, pp. 3055–3065, 2007.

[8] N. P. Rajamane, M. C. Nataraja, J. K. Dattatreya, N. Lakshmanan, and D. Sabitha, "Sulphate resistance and eco-friendliness of geopolymer concretes," *Indian Concrete Journal*, vol. 86, no. 1, pp. 13–22, 2012.

[9] W. G. Valencia Saavedra, D. E. Angulo, and R. Mejía de Gutiérrez, "Fly ash slag geopolymer concrete: Resistance to sodium and magnesium sulfate attack," *Journal of Materials in Civil Engineering*, vol. 28, no. 12, Article ID 04016148, 2016.

[10] S. Thokchom, P. Ghosh, and S. Ghosh, "Performance of fly ash based geopolymer mortars in sulphate solution," *Journal of Engineering Science and Technology Review*, vol. 3, no. 1, pp. 36–40, 2010.

[11] Z. Baščarević, M. Komljenović, Z. Miladinović, V. Nikolić, N. Marjanović, and R. Petrović, "Impact of sodium sulfate solution on mechanical properties and structure of fly ash based geopolymers," *Materials and Structures*, vol. 48, no. 3, pp. 683–697, 2014.

[12] I. Ismail, S. A. Bernal, J. L. Provis, S. Hamdan, and J. S. J. Van Deventer, "Microstructural changes in alkali activated fly ash/slag geopolymers with sulfate exposure," *Materials and Structures/Materiaux et Constructions*, vol. 46, no. 3, pp. 361–373, 2013.

[13] P. Duan, C. Yan, and W. Zhou, "Influence of partial replacement of fly ash by metakaolin on mechanical properties and microstructure of fly ash geopolymer paste exposed to sulfate attack," *Ceramics International*, 2015.

[14] S. Thokchom, P. Ghosh, and S. Ghosh, "Effect of Na 2O content on durability of geopolymer pastes in magnesium sulfate solution," *Canadian Journal of Civil Engineering*, vol. 39, no. 1, pp. 34–43, 2012.

[15] P. Chindaprasirt, U. Rattanasak, and S. Taebuanhuad, "Resistance to acid and sulfate solutions of microwave-assisted high calcium fly ash geopolymer," *Materials and Structures/Materiaux et Constructions*, vol. 46, no. 3, pp. 375–381, 2013.

[16] J. Gao, Z. Yu, L. Song, T. Wang, and S. Wei, "Durability of concrete exposed to sulfate attack under flexural loading and drying-wetting cycles," *Construction and Building Materials*, vol. 39, no. 2, pp. 33–38, 2013.

[17] L. Jiang and D. Niu, "Study of deterioration of concrete exposed to different types of sulfate solutions under drying-wetting cycles," *Construction and Building Materials*, vol. 117, pp. 88–98, 2016.

[18] M. Sahmaran, T. K. Erdem, and I. O. Yaman, "Sulfate resistance of plain and blended cements exposed to wetting-drying and heating-cooling environments," *Construction and Building Materials*, vol. 21, no. 8, pp. 1771–1778, 2007.

[19] G. Lavanya and J. Jegan, "Durability Study on High Calcium Fly Ash Based Geopolymer Concrete," *Advances in Materials Science and Engineering*, vol. 2015, Article ID 731056, 2015.

[20] F. Ming, Y.-S. Deng, and D.-Q. Li, "Mechanical and Durability Evaluation of Concrete with Sulfate Solution Corrosion," *Advances in Materials Science and Engineering*, vol. 2016, Article ID 6523878, 2016.

[21] D. M. J. Sumajouw, S. E. Wallah, and D. Hardjito, "On the Development of Fly Ash-Based Geopolymer Concrete," *Aci Mater J*, vol. 101, no. 6, pp. 467–472, 2004.

[22] X. S. Shi, F. G. Collins, X. L. Zhao, and Q. Y. Wang, "Mechanical properties and microstructure analysis of fly ash geopolymeric recycled concrete," *Journal of Hazardous Materials*, vol. 237-238, pp. 20–29, 2012.

[23] B. Qi, J. Gao, F. Chen, and D. Shen, "Evaluation of the damage process of recycled aggregate concrete under sulfate attack and

wetting-drying cycles," *Construction and Building Materials*, vol. 138, pp. 254–262, 2017.

[24] E. Gruyaert, P. Van Den Heede, M. Maes, and N. De Belie, "Investigation of the influence of blast-furnace slag on the resistance of concrete against organic acid or sulphate attack by means of accelerated degradation tests," *Cement and Concrete Research*, vol. 42, no. 1, pp. 173–185, 2012.

[25] J. Geng, D. Easterbrook, L.-Y. Li, and L.-W. Mo, "The stability of bound chlorides in cement paste with sulfate attack," *Cement and Concrete Research*, vol. 68, pp. 211–222, 2015.

[26] N. Patsikas, N. Katsiotis, P. Pipilikaki, D. Papageorgiou, E. Chaniotakis, and M. Beazi-Katsioti, "Durability of mortars of white cement against sulfate attack in elevated temperatures," *Construction and Building Materials*, vol. 36, no. 4, pp. 1082–1089, 2012.

[27] N. Garg, K. Wang, and S. W. Martin, "A Raman spectroscopic study of the evolution of sulfates and hydroxides in cement-fly ash pastes," *Cement and Concrete Research*, vol. 53, no. 53, pp. 91–103, 2013.

[28] D. Ren, C. Yan, P. Duan, Z. Zhang, L. Li, and Z. Yan, "Durability performances of wollastonite, tremolite and basalt fiber-reinforced metakaolin geopolymer composites under sulfate and chloride attack," *Construction and Building Materials*, vol. 134, pp. 56–66, 2017.

[29] D. W. Breck, *Zeolite molecular sieves : structure, chemistry, and use*, Wiley, 1974.

[30] W. G. Valencia Saavedra and R. Mejía de Gutiérrez, "Performance of geopolymer concrete composed of fly ash after exposure to elevated temperatures," *Construction and Building Materials*, vol. 154, pp. 229–235, 2017.

[31] M. Komljenović, Z. Baščarević, and V. Bradić, "Mechanical and microstructural properties of alkali-activated fly ash geopolymers," *Journal of Hazardous Materials*, vol. 181, no. 1–3, pp. 35–42, 2010.

[32] E. Rozière, A. Loukili, R. Hachem, and F. Grondin, "Durability of concrete exposed to leaching and external sulphate attacks," *Cement and Concrete Research*, vol. 39, no. 12, pp. 1188–1198, 2009.

[33] J. Skalny, V. Johansen, N. Thaulow, and A. Palomo, "DEF: As a form of sulfate attack," *Materiales de Construcción*, vol. 1996, no. 244, pp. 5–29, 1996.

[34] S. A. Bernal and J. L. Provis, "Durability of alkali-activated materials: Progress and perspectives," *Journal of the American Ceramic Society*, vol. 97, no. 4, pp. 997–1008, 2014.